Conformational Studies of Stereoisomeric Tetrols Derived from *syn*- and *anti*-Dibenzo[*a,l*]pyrene Diol Epoxides

Ryszard Jankowiak,*[,†] Freek Ariese,[‡,||] Dan Zamzow,[‡] Andreas Luch,[§,⊥] Heiko Kroth,[§] Albrecht Seidel,[§] and Gerald J. Small[†,‡]

Ames Laboratory - USDOE and Department of Chemistry, Iowa State University, Ames, Iowa 50011, and Institute of Toxicology, University of Mainz, D-55131 Mainz, Germany

Received December 30, 1996[⊗]

An understanding of the conformational behavior of the stereoisomeric tetrols at the 11,12,13,14-positions of dibenzo[*a,l*]pyrene (DB[*a,l*]P) is essential for the spectroscopic identification of DNA adducts derived from the biologically highly active fjord region *syn*- and *anti*-DB[*a,l*]P-11,12-diol 13,14-epoxides. Conformational effects are expected to play an important role in DNA−DB[*a,l*]P diol epoxide reactivity, base-sequence specificity, and conformation dependent repair. The results of conformational studies on *trans-anti*-, *cis-anti*-, and *cis-syn*-DB[*a,l*]P tetrol isomers are presented and compared to the results obtained previously for *trans-syn*-DB[*a,l*]P tetrol (*Carcinogenesis* **17**, 829−837, 1996). Molecular mechanics, dynamical simulations, and semiempirical calculations of electronic transitions are used to interpret the low-temperature fluorescence spectra and ^{1}H NMR data. Molecular dynamics simulations (*in vacuo*) identified two conformers (I and II) for each of the tetrol isomers; in all conformations the aromatic ring system is severely distorted. Fluorescence line-narrowing (FLN) spectroscopy identified two distinct conformational species for the *trans-anti* isomer, one occurring in ethanol and the other occurring in a glycerol/water matrix. The corresponding structures are assigned based on the $S_1 \leftarrow S_0$ transition energies calculated for conformers I and II, respectively. ^{1}H NMR spectroscopy confirmed the structure of conformer I at room temperature. In contrast to *trans-syn*-DB[*a,l*]P tetrol (where the major conformation was identified as a boat structure), both conformations of *trans-anti*-DB[*a,l*]P tetrol feature a half-chair structure for the cyclohexenyl ring with different orientations of the hydroxyl groups. For *cis-anti*- and *cis-syn*-DB[*a,l*]P tetrols, only a single conformer is detected by FLN spectroscopy. The NMR results for the latter appear to be most consistent with a mixture of two half-chair conformers I and II, while for the *cis-anti* isomer a flattened, boatlike conformation was observed. The generally good agreement between the NMR coupling constants and those estimated theoretically indicates that these structures should serve as good starting points for spectroscopic or computational studies of DNA adducts derived from DB[*a,l*]P diol epoxides.

Introduction

Polycyclic aromatic hydrocarbons (PAHs)[1] are a group of environmental pollutants, some of which are strongly carcinogenic. One of the most potent PAH carcinogens presently known is dibenzo[*a,l*]pyrene (DB[*a,l*]P), which has been identified in river sediments (*1*) and in indoor (*2*) and outdoor (*3*) air samples, suggesting potential (eco)-toxicological hazards. Recent *in vivo* studies with rodents have shown that at low doses the tumor-initiating activity of DB[*a,l*]P is significantly greater than that of benzo[*a*]pyrene or 7,12-dimethylbenz[*a*]anthracene (*4*−*6*). DB[*a,l*]P, like other PAHs, can be enzymatically activated to electrophilic intermediates that bind to DNA (*7, 8*); formation of covalent DNA adducts is believed to be responsible for the mutagenic and carcinogenic activity of DB[*a,l*]P (*7, 9, 10*). ^{32}P-Postlabeling analysis of DB-[*a,l*]P−DNA adducts has shown that metabolic activation of DB[*a,l*]P in cell cultures occurs via formation of the fjord region 11,12-diol 13,14-epoxide (DE) intermediates, which can in principle exist in four different stereoisomeric forms (*4, 11*). In addition, both the (±)-*syn*- and (±)-*anti*-DB[*a,l*]PDEs are metabolically formed *in vitro* from DB[*a,l*]P or its 11,12-diol, the precursor of the fjord region diol epoxides, using microsomes from 3-methylcholanthrene-treated rats (*7*). The reaction of the DB-[*a,l*]PDE generated under these conditions with calf thymus DNA (*7*) or the direct reaction with purine bases (*12, 13*) has been demonstrated to form a mixture of stable and depurinating adducts: reaction with the exocyclic amino group of adenine or guanine leads to the

* To whom correspondence should be addressed at Ames Laboratory - USDOE. E-mail: jankowiak@ameslab.gov.
† Ames Laboratory - USDOE.
‡ Department of Chemistry.
§ Institute of Toxicology.
|| Present address: Institute for Environmental Studies, De Boelelaan 1115, NL-1081 HV Amsterdam, The Netherlands.
⊥ Present address: Technical University of Munich, Institute of Toxicology and Environmental Hygiene, Lazarettstrasse 62, D-80636 Munich, Germany.
⊗ Abstract published in *Advance ACS Abstracts,* May 1, 1997.
[1] Abbreviations: CI, configuration interaction; DB[*a,l*]P, dibenzo-[*a,l*]pyrene; DB[*a,l*]PDE-14-N7Ade, 14-(adenin-7-yl)-11,12,13-trihydroxy-11,12,13,14-tetrahydrodibenzo[*a,l*]pyrene; DB[*a,l*]PDE-14-N7Gua, 14-(guanin-7-yl)-11,12,13-trihydroxy-11,12,13,14-tetrahydrodibenzo-[*a,l*]pyrene; DB[*a,l*]P tetrol, 11,12,13,14-tetrahydroxy-11,12,13,14-tetrahydrodibenzo[*a,l*]pyrene; DE, diol epoxide; DMSO, dimethyl sulfoxide; FLN, fluorescence line-narrowing; MM, molecular mechanics; NLN, non-line-narrowing; PAH, polycyclic aromatic hydrocarbon; S_0 state, electronic ground state; S_1 state, lowest excited singlet state.

S0893-228x(96)00211-1 CCC: $14.00

formation of stable adducts (*12, 13*), while binding at the N3- or N7-position of adenine or the N7-position of guanine yields depurinating adducts (*7*). An alternate pathway of microsomal activation of DB[*a,l*]P is a one-electron oxidation, which yields radical cations that can covalently bind to purine bases (*7, 14*).

Low-temperature fluorescence spectroscopy has proven to be a valuable tool for the characterization of various PAH−DNA adducts and PAH metabolites. Fluorescence line-narrowing spectroscopy (FLNS) can be used for fingerprint identification (*15−18*), and the combination of FLNS and non-line-narrowing (NLN) fluorescence spectroscopy provides conformational information (*19−21*). The low-temperature fluorescence spectra of *trans-syn*-DB[*a,l*]P tetrol and the *trans-syn*-DB[*a,l*]PDE-14-N7Ade adduct each showed two distinct fluorescence (0,0) or origin bands having different excited-state vibrational frequencies, as determined by FLNS (*22*). Exploration of the conformational space by molecular modeling and molecular dynamics simulations produced two potential energy minima for each compound, both corresponding to structures in which the aromatic ring system is severely distorted from planarity. For the major conformation I of the adduct, the adenine base is in a pseudoaxial position and the cyclohexenyl ring adopts a half-boat structure. In conformation II, the distal ring is bent in the opposite direction (away from the base), allowing the cyclohexenyl ring to adopt a half-chair structure with the base in a pseudoequatorial position, partially stacked over the distal ring (*22*). The difference in calculated (0,0) transition energies for the two conformers agreed very well with the spectroscopic data, and the relative orientations of the hydrogen atoms bound to the cyclohexenyl ring in the major (half-boat) conformation I were in full agreement with the experimentally-observed ^{1}H NMR coupling constants of *trans-syn*-DB[*a,l*]P tetrol (*22*).

Preliminary laser-induced fluorescence and ^{1}H NMR studies of stable adducts and tetrols from *anti*- and *syn*-DB[*a,l*]PDE also indicated the existence of two molecular conformations. Some stereoisomers showed two distinct fluorescence origin bands having relative intensities that were solvent dependent. These conformational effects render the spectroscopic characterization of these compounds extremely complex. Therefore, a thorough understanding of the conformational behavior of these compounds is needed before one can attempt to unravel the nature of DB[*a,l*]P−DNA adducts formed in *in vitro* and *in vivo* experiments. Furthermore, the conformational preference of a stable adduct will also determine how it is embedded in the DNA helix, and several studies have provided evidence that conformational effects strongly influence the mutagenic activity and repairability of PAH−DNA lesions (*23−25*).

In this paper, our investigations of the conformational characteristics of *trans-anti-*, *cis-anti-*, and *cis-syn*-DB-[*a,l*]P tetrol will be presented. The results will be compared to those obtained earlier for *trans-syn*-DB[*a,l*]P tetrol (*22*). Theoretical calculations, including molecular mechanics, dynamical simulations, and semiempirical calculations of electronic transitions, are used to interpret the ^{1}H NMR data and the low-temperature fluorescence spectra. An understanding of the conformational behavior of these stereoisomeric DB[*a,l*]P tetrols will be important for the spectroscopic identification of adducts from *syn*- and *anti*-DB[*a,l*]P diol epoxides, and it may also provide insight into their biological effects.

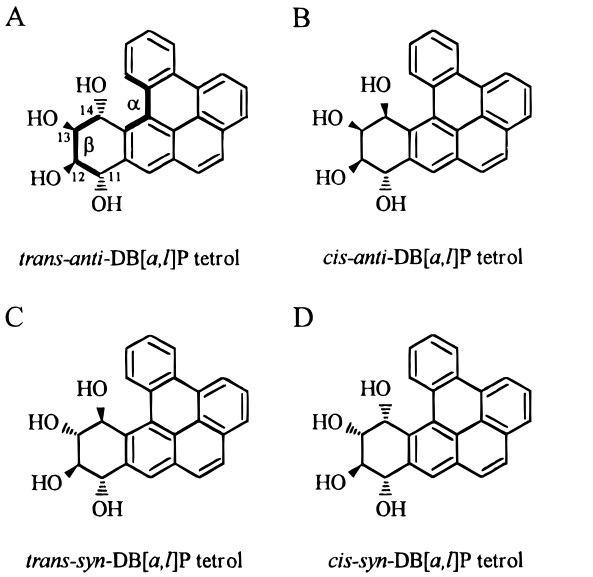

Figure 1. Molecular structures of the four DB[*a,l*]P tetrols investigated: (A) 11*r*,12*t*,13*t*,14*c*-tetrahydroxytetrahydrodibenzo[*a,l*]pyrene, (B) 11*r*,12*t*,13*t*,14*t*-tetrahydroxytetrahydrodibenzo[*a,l*]pyrene, (C) 11*r*,12*t*,13*c*,14*t*-tetrahydroxytetrahydrodibenzo-[*a,l*]pyrene, and (D) 11*r*,12*t*,13*c*,14*c*-tetrahydroxytetrahydrodibenzo[*a,l*]pyrene. Samples were racemic mixtures (only one stereoisomer is shown). The dihedral angles α and β will be used to describe the deviation from planarity in the fjord region and the conformation of the cyclohexenyl ring, respectively.

Experimental Procedures

Caution: *anti- and syn-DB[a,l]P diol epoxides are extremely hazardous chemicals and should be handled carefully in accordance with NIH guidelines.*

Sample Preparation. Molecular structures of the four stereoisomeric DB[*a,l*]P tetrols, namely, *trans-anti-*, *cis-anti-*, *trans-syn-*, and *cis-syn*-DB[*a,l*]P tetrol, are shown in Figure 1. These compounds were obtained by hydrolysis of the synthetically available fjord region *anti-* and *syn*-DB[*a,l*]P diol epoxides[2] and separated by means of reversed-phase HPLC. However, the yield of *cis-anti* tetrol was too low for NMR characterization using this approach. Instead, stereoselective dihydroxylation of DB[*a,l*]P-11,12-dihydrodiol using osmium tetraoxide, according to a procedure described by Bushman et al. (*26*) for other *trans* dihydrodiols, provided *cis-anti*-DB[*a,l*]P tetrol as a white solid in 67% yield: mp 232 °C; ^{1}H NMR (DMSO-d_6/acetone-d_6/D_2O) δ 9.12 (d, 1H, H_1, $J_{1,2} = 7.8$ Hz), 8.99 (d, 1H, H_5, $J_{5,6} = 7.8$ Hz), 8.93 (d, 1H, H_4, $J_{3,4} = 8.1$ Hz), 8.40 (s, 1H, H_{10}), 8.24 (d, 1H, H_7, $J_{6,7} = 7.8$ Hz), 8.10 (AB system, 2H, $H_{8,9}$, $J_{8,9} = 9.0$ Hz), 8.03 (pseudo-t, 1H, H_6), 7.77 (pseudo-t, 1H, H_3), 7.72 (pseudo-t, 1H, H_2), 5.53 (d, 1H, H_{14}, $J_{13,14} = 2.5$ Hz), 5.47 (d, 1H, H_{11}, $J_{11,12} = 5.7$ Hz), 3.83 (pseudo-t, 1H, H_{13}, $J_{12,13} = 6.1$ Hz); FD-MS m/z 370 (M^+, 100).

Low-Temperature Fluorescence Spectroscopy. NLN fluorescence spectra at $T = 77$ K and FLN spectra ($S_1 \leftarrow S_0$ excitation) at $T = 4.2$ K were obtained using a Lambda Physik FL-2002 dye laser pumped by a Lambda Physik Lextra 100 XeCl excimer laser as the excitation source. For FLN several excitation wavelengths were used, each revealing a portion of the S_1 excited-state vibrational frequencies of the analyte. NLN spectra were obtained using nonselective excitation at 308 nm (attenuated excimer laser). Samples were cooled in a glass cryostat with quartz optical windows. Fluorescence was dispersed by a McPherson 2061 1 m focal length monochromator and detected by a Princeton Instruments IRY 1024/G/B intensified photodiode array. For time-resolved detection, a Princeton Instruments FG-100 pulse generator was employed; the detector

[2] Luch, A., Platt, K. L., Seidel, A. Synthesis of fjord region tetrols and their use in hepatic biotransformation studies of dihydrodiols of benzo[*c*]chrysene, benzo[*g*]chrysene and dibenzo[*a,l*]pyrene. *Carcinogenesis*, submitted for publication.

delay time and gate width were set to 45 and 200 ns. For FLN measurements the monochromator was equipped with a 1200 G/mm grating, providing an 18 nm spectral window at 0.1 nm resolution. For low-resolution spectroscopy a 150 G/mm grating was employed, providing a 150 nm window and 0.8 nm resolution. Two solvent matrices of different polarities were used as follows: ethanol or a mixture of glycerol/water (50/50, v/v). Ethanol was spectrophotometric grade from Aldrich; ultrapure grade glycerol was purchased from Spectrum Chemical, Gardena, CA. Solutions (ca. 20 μL) were transferred to quartz tubes (2 mm i.d.) and sealed with a rubber septum. Tetrol concentrations were in the 10^{-7}−(5×10^{-6}) M range. No spectral dependence on concentration or cooling rate was observed.

^{1}H NMR Spectroscopy. ^{1}H NMR spectra were recorded at 298 K on a Bruker AM 400 instrument (Bruker, Karlsruhe, Germany) operating at 400 MHz. Chemical shifts in ppm (δ) are reported elsewhere.[2] DB[*a*,*l*]P tetrols were dissolved in 0.5 mL of a mixture of DMSO-d_6 and acetone-d_6 (4:1, v:v) to which 1 drop of D_2O was added.

Molecular Modeling and Theoretical Calculations. 1. Molecular Mechanics. Conformational analyses were carried out utilizing methods of molecular mechanics (MM), wherein energy calculations were performed with HyperChem's molecular modeling program (release 4.5 for Windows Hypercube Inc., Waterloo, Ontario, Canada). HyperChem's force field parameters describing an "all atom" force field (MM+) developed for organic molecules, which is an extension of the MM2 method (*27, 28*), were employed. Default parameters were used.

As starting structures, different model-built configurations in which the saturated ring was in either a half-chair or a half-boat conformation were used. The Polak−Ribiere algorithm (the conjugate gradient method, *in vacuo*) was used for molecular mechanics optimization; the structures were refined until the rms gradient was less than 0.001 kcal/mol. In the calculations the electrostatic contributions were evaluated from defining a set of bond dipole moments associated with polar bonds.

2. Molecular Dynamics. In the simulations the molecular starting structures, refined by geometry optimization as described above, were used. To calculate thermodynamically-favored conformations, separated from MM structures by energy barriers, quenched dynamics (simulated annealing) was used to explore the conformational space. No constraints were used during high-temperature searches of the conformational space. The starting half-chair and half-boat structures were minimized and then subjected to 20 ps of molecular dynamics at various temperatures between 300 and 400 K. Starting and final temperatures in a dynamic run were set to 0 K, and the heat and cool times were set to 2 (or 5) ps; the step size was 0.0005 ps. At various time points during the simulation approximately 60 randomly-selected structures were also annealed to 0 K and optimized. These optimized structures were subsequently used as starting points for further calculations. All simulations were performed *in vacuo*. The two dihedral angles α and β, defining the distortion in the fjord region and the conformation of the cyclohexenyl ring, as shown in Figure 1, were used as variables during the exploration of the conformational space. Optimization was restricted to the ground states, since only minor geometry changes between the S_0 and S_1 states of large PAH molecules are expected.

3. Semiempirical Quantum Mechanical Calculations of (0,0) Transitions. To aid in interpretation of the observed energy differences between the (0,0) bands of different tetrol conformations, semiempirical quantum mechanical calculations for the low-energy conformations determined above were performed. HyperChem's ZINDO/S method, parameterized to reproduce UV−visible spectroscopic transitions using a configuration interaction (CI) treatment with 130 singly-excited configurations, was applied. The CI space was truncated by considering only the 10 lowest singly-excited configurations. It was assumed that, in first approximation, this approach would describe our systems with sufficient accuracy, since we were interested in the relative energy differences between the $S_1 \leftarrow S_0$ electronic transitions rather than in the absolute values. For spectra and orbital eigenvalues, overlap weighting factors of 1.267 for $\sigma-\sigma$ (*29*) and 0.585 for $\pi-\pi$ (*30, 31*) were used.

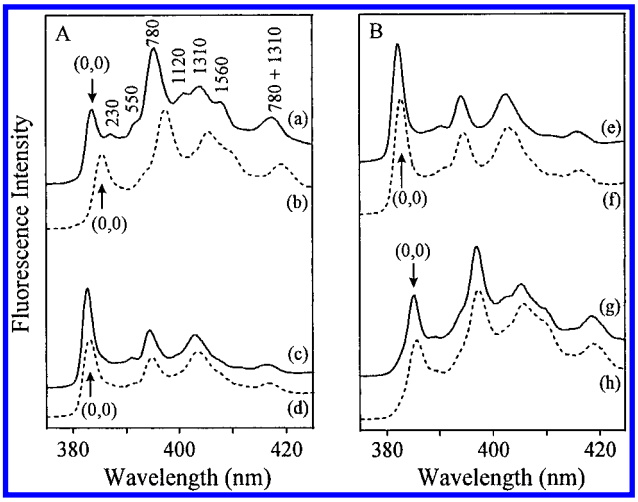

Figure 2. NLN fluorescence spectra for DB[*a*,*l*]P tetrols in ethanol (solid lines) and in 50/50 glycerol/water (dashed lines); $T = 77$ K, 308 nm excitation: (spectra a and b) *trans-anti*-DB[*a*,*l*]P tetrol, (spectra c and d) *cis-anti*-DB[*a*,*l*]P tetrol, (spectra e and f) *trans-syn*-DB[*a*,*l*]P tetrol, and (spectra g and h) *cis-syn*-DB[*a*,*l*]P tetrol.

Table 1. Fluorescence Origin Bands of DB[*a*,*l*]P Tetrols in Ethanol and in Glycerol/Water Matrices[a]

DB[*a*,*l*]P tetrol	(0,0) band I (nm)		(0,0) band II (nm)	
	ethanol	glycerol/water	ethanol	glycerol/water
trans-anti	383.6	*b*	*b*	385.4
cis-anti	382.8	383.2	*b*	*b*
trans-syn[c]	382.2	382.7	*b*	387.0
cis-syn	385.2	385.5	*b*	*b*

[a] $T = 77$ K, $\lambda_{ex} = 308$ nm. [b] Not observed. [c] Data from ref 22.

Results and Discussion

Non-Line-Narrowing Fluorescence Spectra. 1. Tetrols Derived from *anti*-DB[*a*,*l*]PDE. Fluorescence spectra obtained at 77 K in ethanol (solid lines) and in glycerol/water (dashed lines) are shown in Figure 2. The wavelengths of the (0,0) bands are given in Table 1. The labeling of the (0,0) bands in Table 1 as I or II is meant to indicate that they are associated with different molecular conformations. The existence of one or two conformations for each stereoisomeric tetrol was determined mainly on the basis of the FLN spectra, *vide infra*. Before considering the solvent dependence of the tetrol fluorescence spectra, it is important to comment on the vibronic bands which build on the (0,0) band. The ground-state vibrational frequencies are given in spectrum a of Figure 2. The frequencies in spectra b−h are identical within experimental uncertainty, although in some of the spectra the intensities of the relatively weak 230, 550, and 1120 cm^{-1} bands are suppressed. Such variation in intensity is not surprising given that the parent fluorophore B[*e*]P has C_{2v} symmetry, so the out-of-plane deformation depends significantly on the stereochemistry of the tetrol, *vide infra*. Given this, the structure of the spectra in Figure 2 is that expected for B[*e*]P (*32*), which has a characteristic Herzberg−Teller vibronic origin band at 780 cm^{-1}. The intensity of the Herzberg−Teller band for B[*e*]P in a glycerol/water glass is equal to that of the (0,0) band (*32*−*34*). Its significant intensity, derived from the electronic vibrational coupling

Table 2. Calculated Ground-State Energies and Calculated and Observed (0,0) Transition Energies for DB[*a,l*]P Tetrols[a]

DB[*a,l*]P tetrol	conformer	energy (kcal/mol)[b]	oscillator strength	λ_{calc}(0,0) (nm)	λ_{obs}(0,0) (nm)[c]
trans-anti	I*	−2.2	0.006	383.2	383.6 (EtOH)
	II	−2.0	0.002	384.4	385.4 (g/w)
cis-anti	I	−0.6	0.004	382.0	382.8 (EtOH) 383.2 (g/w)[d]
	I′ *	−0.2	0.004	382.8	
	II	−3.4	0.004	384.3	
trans-syn[e]	I*	−1.0	0.009	381.4	382.2 (EtOH) 382.7 (g/w)
	II	−3.5	0.008	384.0	387.0 (g/w)
cis-syn	I*	−3.2	0.005	382.2	
	II	−2.2	0.004	384.5	385.2 (EtOH) 385.5 (g/w)

[a] The conformation denoted by an asterisk is the most consistent with the room temperature ^{1}H NMR data. [b] Ground-state energy minimum in isolation (no solvent). [c] Spectroscopically-observed (0,0) transition energies in ethanol (EtOH) or glycerol/water (g/w) at 77 K. [d] The observed fluorescence origin bands may correspond to either the I or the I′ conformation. [e] Data from ref 22.

between the S_1 state and higher energy dipole-allowed states (*34*), is a consequence of the $S_1 \leftarrow S_0$ absorption transition being only weakly allowed, Table 2. However, the allowedness depends on deviations from C_{2v} symmetry, and thus, one expects to observe a dependence of the intensity of the Herzberg−Teller band relative to that of the allowed (0,0) band on stereochemistry, as seen in Figure 2.

Concerning the aforementioned solvent dependence there is, for *trans-anti*-DB[*a,l*]P tetrol (Figure 2A, a and b), a relatively large shift in the position of the (0,0) band. In ethanol the origin band is located at 383.6 nm, while in glycerol/water it is at 385.4 nm. For *cis-anti*-DB[*a,l*]P tetrol (Figure 2A, c and d) the shift of the (0,0) band is relatively small. Its position in ethanol is 382.8 nm, while in glycerol/water it is 383.2 nm. In addition, its (0,0) band is now the most intense feature, unlike *trans-anti*-DB[*a,l*]P tetrol for which the Herzberg−Teller origin band at 780 cm^{-1} is most intense. The vibronic features are very similar in the two solvents.

2. Tetrols Derived from *syn*-DB[*a,l*]PDE. The spectra for the *trans-syn* isomer (Figure 2B, e and f) resemble those of the *cis-anti* isomer, with the (0,0) band the most intense feature and its position shifting only 0.5 nm to the red on going from ethanol to glycerol/water. As mentioned in the Introduction, spectral characterization of the *trans-syn* isomer has been reported previously (*22*). In that work the FLN spectra revealed that in the glycerol/water matrix there is a minor conformation denoted as II in Table 1. The major conformation in both ethanol and glycerol/water is I. For the *cis-syn* tetrol isomer (Figure 2B, g and h), the 780 cm^{-1} Herzberg−Teller origin band is the most intense spectral feature, as is the case for the *trans-anti* isomer. However, the shift of the (0,0) band of *cis-syn* tetrol on going from ethanol to glycerol/water solvent is small, 0.3 nm.

The NLN fluorescence spectra shown in Figure 2 provide very interesting information. For instance, they reveal that in the case of *trans-anti*- and *cis-syn*-DB[*a,l*]P tetrol the (0,0) transition is relatively weak, as expected for molecules bearing a B[*e*]P chromophore, while the (0,0) transition appears much more allowed in the case of *cis-anti*- and *trans-syn*-DB[*a,l*]P tetrol. This effect must be due to a deviation from C_{2v} symmetry that is apparently much stronger in the conformations adopted

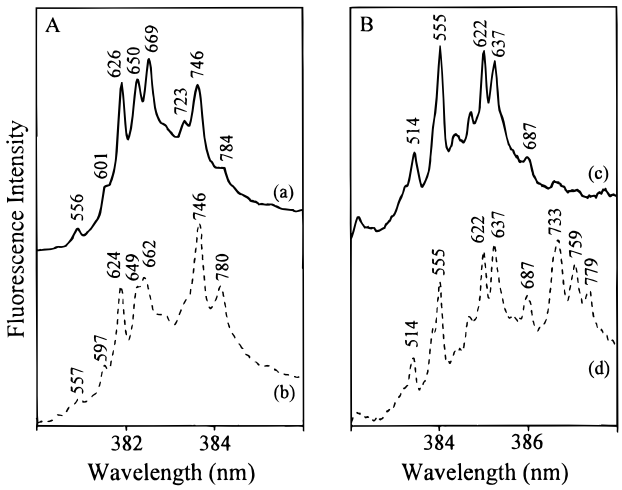

Figure 3. Frame A: FLN spectra for *cis-anti*-DB[*a,l*]P tetrol in (a) ethanol and (b) 50/50 glycerol/water; laser excitation at 373.0 nm. Frame B: FLN spectra for *cis-syn*-DB[*a,l*]P tetrol in (c) ethanol and (d) 50/50 glycerol/water; laser excitation at 376.0 nm; $T = 4.2$ K. The FLN peaks are labeled with their excited-state vibrational frequencies, in cm^{-1}.

by the latter two compounds. In order to obtain more information regarding the molecular conformations of the tetrols, we turned to FLN spectroscopy coupled with computational chemistry and NMR spectroscopy.

Vibronically-Excited FLN Spectra. Vibronically-excited FLN spectroscopy is a powerful technique for analysis of the vibrational structure of excited electronic states of molecular species, including PAH−DNA adducts (*15*−*17*, *19*−*23*, *25*). A nonmathematical discussion of the principles is given in ref 15. The approach and reasoning that follow are based mainly on ref 22. The results for the *cis-anti* and *cis-syn* isomers are considered first since they are of the type expected when only one conformation is present, and it is the same in the two glass hosts.

The FLN multiplet origin structures for the *cis-anti* isomer in ethanol (solid line, a) and in glycerol/water (dashed line, b) are shown in Figure 3A. The same excitation wavelength, 373.0 nm, was used for both glasses since the (0,0) bands are displaced from each other by only 0.4 nm, Table 1. This wavelength excites vibrations of the S_1 state with frequencies in the 550−800 cm^{-1} region. The FLN bands are labeled with their S_1 vibrational frequencies in cm^{-1}. The vibrational frequencies in the two glasses are very similar (±3 cm^{-1} uncertainty). The intensity distributions are also similar, with the higher relative intensities of the 746 and 780 cm^{-1} modes in glycerol/water explicable in terms of the 0.4 nm red shift of the (0,0) band relative to ethanol, Table 1. If two molecular conformations existed and contributed to the (0,0) bands of spectra c and d in Figure 2 or if the (0,0) bands in ethanol and glycerol/water were due to different conformations, one would not expect the striking similarity between spectra a and b in Figure 3. This point was emphasized in ref 22 and will become clearer when the results for the *trans-anti* isomer are considered. We conclude that there is only one dominant conformation and that its structure is not significantly different in the two solvents.

The conclusions for the *cis-syn* isomer, based on FLN spectra c and d of Figure 3B, are the same. For these spectra an excitation wavelength of 376.0 nm was used. Again, the vibrational frequencies in the two glasses are

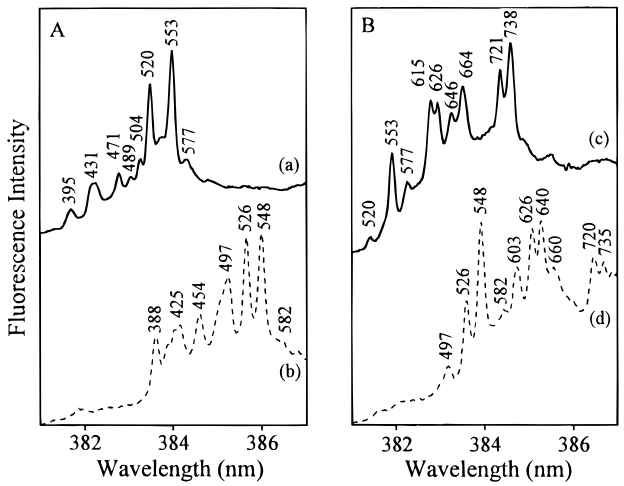

Figure 4. FLN spectra for *trans-anti*-DB[*a,l*]P tetrol in (a and c) ethanol and (b and d) 50/50 glycerol/water; $T = 4.2$ K. Laser excitation wavelengths are 376.0, 378.0, 374.0, and 376.0 nm, respectively, for spectra a−d. The FLN peaks are labeled with their excited-state vibrational frequencies, in cm^{-1}. Due to the red shift of the origin band of *trans-anti*-DB[*a,l*]P tetrol in glycerol/water compared to ethanol (see Figure 2), different laser wavelengths were used in order to excite similar vibrational modes with approximately the same efficiency.

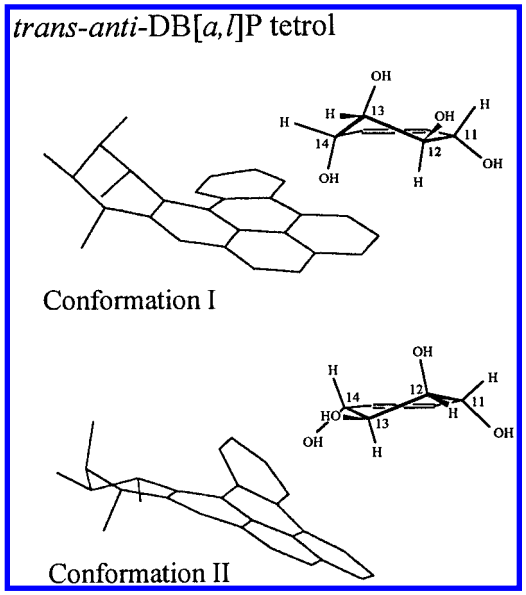

Figure 5. Optimized 0 K ground-state structures of *trans-anti*-DB[*a,l*]P tetrol obtained after simulated annealing. Two different half-chair conformers (I and II) are presented; hydrogen atoms are omitted for clarity. The insets show the conformation of the cyclohexenyl ring in more detail (fjord region is on the left).

very similar. The higher relative intensities of the higher frequency modes in spectrum d for glycerol/water are due to the (0,0) band in this solvent being red-shifted by 0.3 nm relative to ethanol, Table 1, as well as its greater inhomogeneous broadening (compare the widths of the (0,0) bands of spectra g and h in Figure 2).

We consider next the *trans-anti*- and *trans-syn*-DB-[*a,l*]P tetrols. FLN spectra are shown in Figure 4 for the *trans-anti* isomer with a and c obtained in ethanol and b and d in glycerol/water. Frames A and B correspond to different excitation wavelengths (λ_{ex}) which expose different regions of the vibronic spectrum. For ethanol, spectra for $\lambda_{ex} = 376.0$ and 374.0 nm are shown in frames A and B, respectively; for glycerol/water, $\lambda_{ex} = 378.0$ and 376.0 nm spectra are shown. The λ_{ex}-values for glycerol/water are 2 nm higher because the (0,0) band in this solvent is red-shifted by this amount relative to ethanol, Figure 2 and Table 1. That is, it is important that the excitation wavelengths for the two glasses excite the same excited-state vibrational region. Comparison of spectra a and b in Figure 4 reveals that there are significant differences in vibrational frequencies and intensities between ethanol and glycerol/water. This is also the case for spectra c and d. Spectra obtained with other λ_{ex}-values are consistent with this. Thus, the FLN results for the *trans-anti* isomer strongly indicate that its molecular conformations in the two glasses are very different. As mentioned in the Introduction, the same conclusion was reached in ref 22 for the *trans-syn* isomer. In contrast, the FLN spectra in Figure 3 for the *cis-anti* and *cis-syn* isomers are consistent with each of them having the same conformation in the two glasses.

Molecular Modeling and Theoretical Calculations. The FLN spectra shown above and in ref 22 indicate that *trans-anti*- and *trans-syn*-DB[*a,l*]P tetrols adopt distinctly different conformations in ethanol and glycerol/water, while the *cis-anti* and *cis-syn* isomers appear to undergo only a small solvent shift. In order to understand these results, a theoretical investigation was initiated using molecular mechanics and molecular dynamics simulations. Dynamical simulation studies were carried out at temperatures between 300 and 400 K; local minima in the potential energy surface were searched for by simulated rapid cooling of approximately 60 high-temperature structures with subsequent optimization. Several different starting structures were used as follows: half-chair and half-boat structures obtained from molecular mechanics were initially investigated, but in molecular modeling, the optimized structures obtained during simulated annealing were also used as starting points for subsequent simulations. However, at higher temperatures the same conformational equilibrium was reached, regardless of the starting conformation.

1. Tetrols Derived from *anti*-DB[*a,l*]PDE. For *trans-anti*-DB[*a,l*]P tetrol, two different structures were obtained, in agreement with the spectroscopic data. Interestingly, in contrast to *trans-syn*-DB[*a,l*]P tetrol, for which the most stable conformation has been shown to be a half-boat conformation (*22*), the cyclohexenyl ring of the *trans-anti* isomer exists in two different half-chair conformations. The hydroxyl substituent in the fjord region at C_{14} adopts either a semiaxial position (Figure 5, top) or a semiequatorial one (Figure 5, bottom). Both conformations show severe distortion from planarity in the fjord region due to steric crowding (see Table 3) but in opposite directions. In both cases the distal ring is bent away from the semiequatorial substituent and toward the semiaxial substituent at C_{14}. Interconversions at temperatures above 300 K indicate that these conformations are in equilibrium on a picosecond time scale. During the simulations some higher energy conformations were also observed. These structures, however, would always convert to half-chair conformation I or II upon further structure optimization.

Although FLN results for the *cis-anti* isomer indicate the existence of only a single conformation, the simulations yielded two distinct structures, both of which could be trapped at 0 K, Figure 6. As was the case for the *trans-anti* isomer, in both conformations I and II the cyclohexenyl ring adopts a half-chair conformation. In conformation I the OH group at C_{14} is in a semiaxial

Table 3. Dihedral Angles of DB[*a,l*]P Tetrols Calculated for the Various Conformations[a]

DB[*a,l*]P tetrol	conformer	α (deg)	β (deg)	structure assignment[b]
trans-anti	I	−24	60	half-chair, pseudoaxial
	II	27	−63	half-chair, pseudoequatorial
cis-anti	I	24	−59	half-chair, pseudoaxial
	I′	24	−25	flattened, pseudoaxial
	II	−24	63	half-chair, pseudoequatorial
trans-syn[c]	I	25	8	half-boat, pseudoaxial
	II	−26	64	half-chair, pseudoequatorial
cis-syn	I	−24	62	half-chair, pseudoaxial
	II	26	−60	half-chair, pseudoequatorial

[a] α describes the deviation from planarity in the fjord region, and β describes the conformation of the cyclohexenyl ring (see Figure 1). [b] Conformation of the cyclohexenyl ring and orientation of the hydroxyl group at C_{14}. [c] Data from ref 22.

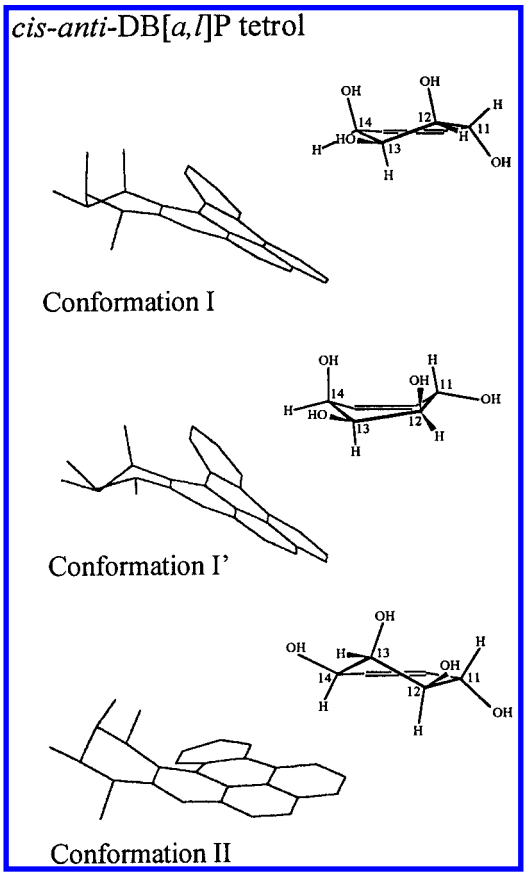

Figure 6. Optimized 0 K ground-state structures of *cis-anti*-DB[*a,l*]P tetrol obtained after simulated annealing. Two different half-chair conformers (I and II) are presented, as well as a flattened, boatlike conformation (I′); hydrogen atoms are omitted for clarity. The insets show the conformation of the cyclohexenyl ring in more detail (fjord region is on the left).

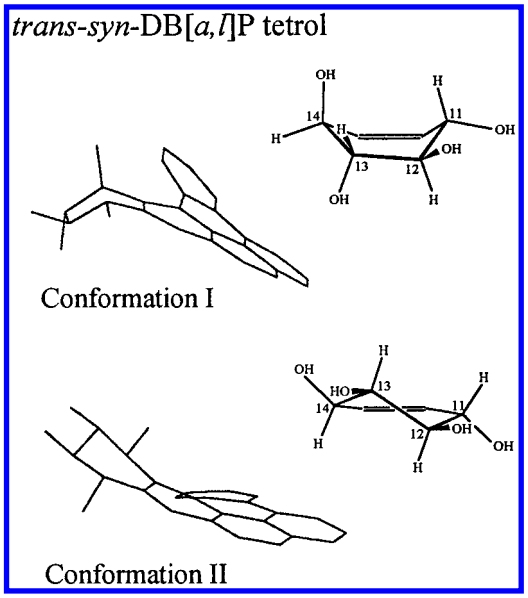

Figure 7. Optimized 0 K ground-state structures of *trans-syn*-DB[*a,l*]P tetrol obtained after simulated annealing. Conformation I is a boatlike structure, and conformation II is a half-chair; hydrogen atoms are omitted for clarity. The insets show the conformation of the cyclohexenyl ring in more detail (fjord region is on the left); data from ref 22.

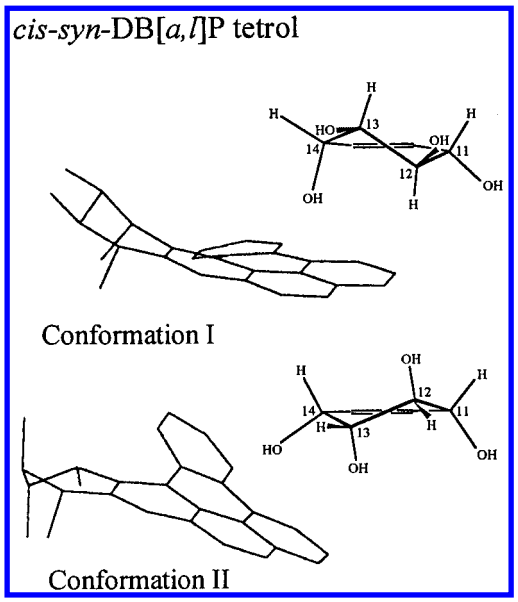

Figure 8. Optimized 0 K ground-state structures of *cis-syn*-DB[*a,l*]P tetrol obtained after simulated annealing. Conformations I and II are both half-chair conformations; hydrogen atoms are omitted for clarity. The insets show the conformation of the cyclohexenyl ring in more detail (fjord region is on the left).

position, while in conformation II its orientation is semiequatorial. In the case of conformation I, a downward movement of C_{12}, flattening the dihedral angle β and changing the conformation of the cyclohexenyl ring from a half-chair to a more boatlike structure, was frequently observed during the simulations. This tendency is presumably caused by diaxial strain between the hydroxyl substituents at C_{12} and C_{14}, but this flattened structure (conformation I′) could not be trapped at 0 K during the simulations. Conformation I′ shown in Figure 6 serves merely to define this motion.

2. Tetrols Derived from *syn*-DB[*a,l*]PDE. Molecular simulations of the *trans-syn* isomer yielded a major conformation I, in which the cyclohexenyl ring adopts a boatlike structure, as well as a minor half-chair conformation II (*22*). For ease of comparison these structures are reproduced here in Figure 7. For the *cis-syn* isomer only a single conformation could be trapped at 0 K, consistent with the FLN results. For this conformation the cyclohexenyl ring adopts a half-chair conformation with the fjord region hydroxyl group in a semiaxial orientation and the distal ring bent away from the semiequatorial hydrogen, as shown in Figure 8 (top). In the high-temperature dynamical simulations another conformation was frequently observed. This structure, conformation II of Figure 8, has its fjord region hydroxyl group in a semiequatorial orientation. In the quenched dynamics experiments conformation II always converted into I. Structural results for the conformations of the four tetrol isomers are summarized in Table 3.

Electronic Transition Calculations. The oscillator strengths and wavelengths (λ_{calc}) of the origin or (0,0) bands calculated using ZINDO/S are given in Table 2 along with the observed λ-values (λ_{obs}). The $S_1 \leftarrow S_0$ absorption transition is only weakly allowed (*32, 33, 35*); the low values for the oscillator strengths given in Table 2 reflect this. Overall, there is remarkably good agreement between the observed and calculated λ-values, better than should be expected given that ZINDO/S is a semiempirical method. The primary motivation was to compare the transition wavelength difference calculated for the two conformations of each tetrol isomer with the experimental value. The largest difference is 2.6 nm or 180 cm^{-1}, calculated for the *trans-syn* isomer. Again, two conformations (one in ethanol and the other in glycerol/water) were observed by FLN only for the *trans-syn* and *trans-anti* isomers. In the second column of Table 2 the asterisk superscript on the conformer designation indicates the conformation most consistent with the room temperature NMR results (DMSO-d_6/acetone-d_6/D_2O solvent), *vide infra*. With this in mind, it is clear that the ground-state energies (*in vacuo*) listed in the third column are of no use in predicting the most stable conformation. They are included only for completeness.

1. Tetrols Derived from *syn*-DB[*a,l*]PDE. We start with the results for the *trans-syn* isomer from ref 22, given here in Table 2. The conformation observed in both ethanol and glycerol/water at 382.2 and 382.7 nm, respectively, was assigned to conformer I rather than II (Figure 7), in part, because of the λ_{calc}-values. The second (minor) conformation, identified only in glycerol/water at 387.0 nm, was assigned as conformer II. A second factor was that the NMR results indicated only a single conformation, one that is most consistent with conformer I, *vide infra*. We recognize that assignment of conformer type on the basis of comparison between the observed and calculated λ-values of the (0,0) band is tenuous given that the ZINDO/S method does not account for solvent dependence. However, the differences in λ-values of the (0,0) bands should be given quite accurately. Therefore, for consistency we continue this procedure in what follows but, in doing so, point out problems when they arise.

For the *cis-syn* isomer, the FLN spectra are consistent with a single conformation, one and the same in both ethanol and glycerol/water with $\lambda_{obs} = 385.2$ and 385.5 nm, respectively. On the basis of the λ_{calc}-values, one would assign the conformation as II (Figure 8). However, the NMR results indicate the presence of two conformations, I and II, *vide infra*.

2. Tetrols Derived from *anti*-DB[*a,l*]PDE. The FLN results for the *trans-anti* isomer indicate that the single conformation in ethanol and the single conformation in glycerol/water are very different. In Table 2 (Figure 5) they are assigned as conformers I and II, respectively, on the basis of the λ_{calc}-values. The NMR results indicate the presence of only one conformation, one consistent with conformer I, *vide infra*. The FLN results for the *cis-anti* isomer indicate the presence of only one conformation, one that is the same in both ethanol and glycerol/water. On the basis of the λ_{calc}-values, one would assign it as conformer I (Figure 6). However, the NMR data are most consistent with a slightly-flattened conformer I′ (Figure 6). The calculated energy differences between the ground states of conformers associated with each of the four tetrol isomers in Table 2 are small, of the order of kT at room temperature. For the *cis-anti* isomer, conformer II is predicted to lie lower than I by 3.2 kcal/mol. However, ZINDO/S is not parameterized for ground-state geometry and energy but, rather, for spectroscopic transitions. Nevertheless, the assignment of the FLN-detected conformation to I should not be considered as firm.

Before turning to the NMR results, we consider whether the vibrational intensity distributions in the NLN fluorescence spectra of Figure 2, together with ZINDO/S results, provide any guidance for conformer assignment. The oscillator strengths given in Table 2 were calculated for frozen ground-state geometries as determined by the molecular dynamics simulations. Thus, they do not include the contribution from vibronic coupling. Rather, they reflect the dipole strength of the (0,0) band and the Franck−Condon modes that build on it. A reasonable first approach to the question posed is to assume that the intensity of the 780 cm^{-1} band is independent of isomer and conformation and to use the oscillator strengths given in Table 2 to predict the ratios of the intensity of the (0,0) band to the 780 cm^{-1} band and compare them against the experimental values. We have done so and find that the agreement is poor. The easiest way to see this is to compare the spectra for the *cis-anti* isomer (Figure 2A, c and d) with those for the *trans-syn* isomer (Figure 2B, e and f). The above intensity ratio values for all four spectra are nearly identical, while the oscillator strength for the former isomer is a factor of 2 smaller than that of the latter. Thus, the answer to the question is no. An understanding of the vibrational intensity distributions would require, in part, accurate calculations of the geometries of the ground and S_1 excited electronic states as well as vibronically-induced absorption intensities.

^{1}H NMR Spectroscopy. The formation and NMR characterization of *trans-anti-*, *trans-syn-*, and *cis-syn-*DB[*a,l*]P tetrols have been described previously.[2] ^{1}H NMR spectra of the four stereoisomeric tetrols were acquired in order to determine their preferred conformation in solution at room temperature. The relevant coupling constants of the methine protons CH_{11}, CH_{12}, CH_{13}, and CH_{14} are compiled in Tables 4 and 5. From the set of coupling constants, the dihedral angles between the methine protons were estimated according to the Karplus equation (*35*) and compared to the dihedral angles obtained theoretically for the 0 K optimized structures, Tables 4 and 5.

1. Tetrols Derived from *anti*-DB[*a,l*]PDE. The coupling constants obtained for *trans-anti*-DB[*a,l*]P tetrol are $J_{11,12} = 7.6$ Hz, $J_{12,13} = 2.8$ Hz, and $J_{13,14} = 4.4$ Hz. These values are consistent with half-chair conformation I in Figure 5, in which the protons CH_{11} and CH_{12} are in a pseudoaxial/pseudoaxial orientation and the hydroxyl group at CH_{14} is also pseudoaxial. The alternative conformation II would have led to a small coupling constant for the proton pair $CH_{13}-CH_{14}$ and a large coupling constant for the proton pair $CH_{11}-CH_{12}$. Apparently, conformation II does not exist, to any significant extent, in the NMR solvent at room temperature.

The conformation for *cis-anti*-DB[*a,l*]P tetrol which best matches the coupling constants $J_{10,11} = 5.7$ Hz, $J_{12,13} = 6.1$ Hz, and $J_{13,14} = 2.5$ Hz is a half-chair with the hydroxyl group at C_{14} in a pseudoaxial position, flattened at the $C_{11}-C_{12}-C_{13}$ bonds. This would require a relatively small dihedral angle β of about 25−35°, in good accordance with the observed coupling constant $J_{12,13}$ of 6.1 Hz. This is in agreement with the dynamical simula-

Table 4. Calculated Dihedral Angles with Estimated and Experimentally-Observed ^{1}H NMR Coupling Constants for the Proton Pairs J_{ij} of the Cyclohexenyl Ring

A. *trans-anti*-DB[*a,l*]P Tetrol

	conformer I		conformer II		
proton pairs (*i, j*)	calculated angle (deg)	estimated coupling constant[a]	calculated angle (deg)	estimated coupling constant[a]	NMR coupling constant (Hz)[b]
11, 12	−147	large	−72	small	7.6
12, 13	58	small	−63	small	2.8
13, 14	50	small	169	very large	4.4

B. *cis-anti*-DB[*a,l*]P Tetrol

	conformer I		conformer I′ [c]		conformer II		
proton pairs (*i, j*)	calculated angle (deg)	estimated coupling constant[a]	calculated angle (deg)	estimated coupling constant[a]	calculated angle (deg)	estimated coupling constant[a]	NMR coupling constant (Hz)[b]
11, 12	−78	small	−144	medium	−155	large	5.7
12, 13	−61	small	−27	medium	63	small	6.1
13, 14	58	small	61	small	−57	small	2.5

[a] Estimates of coupling constants as a function of dihedral angles, based on Karplus' relation (*35*). [b] NMR spectra were recorded in DMSO-d_6/acetone-d_6/D_2O; data for *trans-anti* tetrol taken from Luch et al.[2] [c] This conformation could not be trapped at 0 K during molecular dynamics simulations (see text).

Table 5. Calculated Dihedral Angles with Estimated and Experimentally-Observed ^{1}H NMR Coupling Constants for the Proton Pairs J_{ij} of the Cyclohexenyl Ring

A. *trans-syn*-DB[*a,l*]P Tetrol

	conformer I		conformer II		
proton pairs (*i, j*)	calculated angle (deg)	estimated coupling constant[a]	calculated angle (deg)	estimated coupling constant[a]	NMR coupling constant (Hz)[b]
11, 12	−169	very large	−155	large	8.9
12, 13	121	small	178	very large	1.8
13, 14	−71	small	−171	very large	2.2

B. *cis-syn*-DB[*a,l*]P Tetrol

	conformer I		conformer II		
proton pairs (*i, j*)	calculated angle (deg)	estimated coupling constant[a]	calculated angle (deg)	estimated coupling constant[a]	NMR coupling constant (Hz)[b]
11, 12	−148	large	−77	small	4.0
12, 13	175	very large	53	small	8.0
13, 14	−62	small	53	small	2.9

[a] Estimates of coupling constants as a function of dihedral angles, based on Karplus' relation (*35*). [b] NMR spectra were recorded in DMSO-d_6/acetone-d_6/D_2O; data taken from Luch et al.[2]

tions in which conformation I of *cis-anti*-DB[*a,l*]P tetrol was found to undergo a similar flattening of the ring at C_{12} to a more boatlike conformation I′, Figure 6.

2. Tetrols Derived from *syn*-DB[*a,l*]PDE. The coupling constants obtained for *trans-syn*-DB[*a,l*]P tetrol ($J_{11,12}$ = 8.9 Hz, $J_{12,13}$ = 1.8 Hz, and $J_{13,14}$ = 2.2 Hz) are fully compatible with the half-boat conformation (conformer I in Figure 7) predicted by dynamical simulations (*22*). A dihedral angle between CH_{12} and CH_{13} of about 90° would be consistent with the exceptionally small coupling constant for $J_{12,13}$. In ref 22, the spectroscopic and theoretical evidence also pointed to a boat structure as the preferential conformer of *trans-syn*-DB[*a,l*]P tetrol.

In the case of *cis-syn*-DB[*a,l*]P tetrol, the large coupling constant $J_{12,13}$ = 8.0 Hz indicates that under the ^{1}H NMR conditions the half-chair conformer I (Figure 8, top frame) is the major conformation. However, the somewhat small coupling constant $J_{11,12}$ (only 4.0 Hz) indicates that at room temperature at least one other conformation contributes to the overall signal, most likely the alternative half-chair conformation II.

Concluding Remarks

The fluorescence line-narrowing and NMR results presented here further establish the importance of dual molecular conformations for the stereoisomers of DB[*a,l*]P tetrol associated with the saturated ring. Molecular dynamics simulations (*in vacuo*) served to identify two conformers (I and II) for each of the four tetrol isomers, Figures 5−8 and Table 3. All conformations show a significant distortion from planarity of the B[*e*]P chromophore, defined by the angle α in Table 3. FLN spectroscopy identified two distinct conformations for the *trans-anti* isomer, one in ethanol and the other in the glycerol/water matrix. They were assigned as conformers I and II, respectively, on the basis of the calculated $S_1 \leftarrow S_0$ transition energies. Both have a half-chair conformation of the cyclohexenyl ring but different orientations of the hydroxyl group at C_{14} (Table 3). The room temperature ^{1}H NMR spectra (DMSO-d_6/acetone-d_6/D_2O solvent) indicate the existence of only conformer I. Thus, it is apparent that solvent plays an important role in determining the energetics of the ground-state conformers. As another example, FLN spectra revealed that,

while the same conformer (assigned as I) for the *trans-syn* isomer is dominant in both ethanol and glycerol/water, a second minor conformer (II) exists in glycerol/water. In this case the conformation of the cyclohexenyl ring of conformers I and II is assigned as half-boat and half-chair, respectively. NMR revealed the existence of only the major conformer I. Only a single one, and the same conformer in both glasses, was detected by FLN for each of the other two isomers, *cis-anti* and *cis-syn*. The NMR results for the *cis-syn* isomer appear to be most consistent with a mixture of conformers I and II. The NMR results for the *cis-anti* isomer indicate the predominance of a flattened, boatlike conformer I′.

It is apparent that molecular dynamics simulations in the presence of solvent are required for a complete understanding of the conformations of the four tetrol isomers. However, the generally good agreement between the NMR coupling constants and those estimated from the structures reported here indicates that these structures should serve as good starting points in future computations. The agreement between the calculated (ZINDO/S) and observed S_1 state energies for the dual conformations of the tetrol isomers is surprisingly good. In particular, the calculations predict that the wavelength shift between the fluorescence origins of conformers I and II for each of the four isomers is small, ∼1-2 nm, as observed. As mentioned above, assignments of FLN-identified conformations as I or II were made on the basis of the calculated transition wavelengths.

These studies were stimulated by our earlier finding that depurinating DNA adducts from *syn*-DB[*a,l*]P diol epoxide can exist in dual conformations (*22*). Conformational effects can be expected to be important in understanding DNA−diol epoxide reactivity, including base-sequence specificity, and the structures of stable DNA adducts formed from the diol epoxides of DB[*a,l*]P and other PAHs with a crowded fjord region. Although extrapolation of our results to conformations of DB[*a,l*]P-derived adducts in aqueous buffer solution or embedded in a DNA helix should be carried out with caution, we note that DB[*a,l*]PDE-derived adducts in intact DNA (in water/buffer solution) exist in multiple conformations.[3] Therefore the present results should be indispensible for future interpretation of spectroscopic data obtained from more complex systems. It is entirely possible that the molecular conformation of the diol epoxide may be important for understanding the bound metabolite's preferences toward external, base-stacked, and intercalated conformations. Recently, it has been shown, for benzo[*a*]pyrene (*25*) and DB[*a,l*]P,[3] that the repair of external adducts is considerably more facile than that for intercalated adducts.

Acknowledgment. This research project was supported by the Office of Health and Environmental Research of the U.S. Department of Energy. Ames Laboratory is operated for the U.S. Department of Energy by Iowa State University under Contract No. W-7405-Eng-82. Partial support from the National Institutes of Health, Grant POI CA49210-05, to F.A. and D.Z. is also acknowledged. The authors thank Dr. E. L. Cavalieri and Dr. K.-M. Li for providing us with the *trans-anti*-, *trans-syn*-, and *cis-syn*-DB[*a,l*]P tetrol samples for the spectroscopic studies.

[3] Jankowiak, R., Ariese, F., Hewer, A., Luch, A., Zamzow, D., Hughes, N. C., Phillips, D., Seidel, A., Platt, K. L., Oesch, F., and Small, G. J. Structure, conformations, and repair of DNA adducts from DB[*a,l*]P: ^{32}P-postlabeling and fluorescence studies. *Chem. Res. Toxicol.*, submitted for publication.

References

(1) Kozin, I. S., Gooijer, C., and Velthorst, N. H. (1995) Direct determination of dibenzo[*a,l*]pyrene in crude extracts of environmental samples by laser-excited Shpol'skii spectroscopy. *Anal. Chem.* **67**, 1623−1626.

(2) Mumford, J. L., Li, X., Hu, F., Lu, X. B., and Chuang, J. C. (1995) Human exposure and dosimetry of polycyclic aromatic hydrocarbons in urine from Xuan Wei, China with high lung cancer mortality associated with exposure to unvented coal smoke. *Carcinogenesis* **16**, 3031−3036.

(3) de Ratt, W. K., Kooijman, S. A. L. M., and Gielen, J. W. J. (1987) Concentrations of polycyclic hydrocarbons in airborne particles in the Netherlands and their correlation with mutagenicity. *Sci. Total Environ.* **66**, 95−114.

(4) Ralston, S. L., Seidel, A., Luch, A., Platt, K. L., and Baird, W. M. (1995) Stereoselective activation of dibenzo[*a,l*]pyrene to (-)-*anti*(11*R*,12*S*,13*S*,14*R*)- and (+)-*syn*(11*S*,12*R*,13*S*,14*R*)-11,12-diol-13,14-epoxides which bind extensively to deoxyadenosine residues of DNA in the human mammary carcinoma cell line MCF-7. *Carcinogenesis* **16**, 2899−2907.

(5) Cavalieri, E. L., Higginbotham, S., RamaKrishna, N. V. S., Devanesan, P. D., Todorovic, R., Rogan, E. G., and Salmasi, S. (1991) Comparative dose-response tumorigenicity studies of dibenzo[*a,l*]pyrene versus 7,12-dimethylbenz[*a*]anthracene, benzo[*a*]pyrene, and two dibenzo[*a,l*]pyrene dihydrodiols in mouse skin and rat mammary gland. *Carcinogenesis* **12**, 1939−1944.

(6) Higginbotham, S., RamaKrishna, N. V. S., Johansson, S. L., Rogan, E. G., and Cavalieri, E. L. (1993) Tumor-initiating activity and carcinogenicity of dibenzo[*a,l*]pyrene versus 7,12-dimethylbenz[*a*]anthracene and benzo[*a*]pyrene at low dose in mouse skin. *Carcinogenesis* **14**, 875−878.

(7) Li, K.-M., Todorovic, R., Rogan, E. G., Cavalieri, E. L., Ariese, F., Suh, M., Jankowiak, R., and Small, G. J. (1995) Identification and quantitation of dibenzo[*a,l*]pyrene-DNA adducts formed by rat liver microsomes *in vitro*: preponderance of depurinating adducts. *Biochemistry* **34**, 8043−8049.

(8) Conney, A. H. (1982) Induction of microsomal enzymes by foreign chemicals and carcinogenesis by polycyclic aromatic compounds. *Cancer Res.* **42**, 4875−4491.

(9) Luch, A., Glatt, H., Platt, K. L., Oesch, F., and Seidel, A. (1994) Synthesis and mutagenicity of the diastereomeric fjord-region 11,12-dihydrodiol 13,14-epoxides of dibenzo[*a,l*]pyrene. *Carcinogenesis* **15**, 2507−2516.

(10) Gill, H. S., Kole, P. L., Wiley, J. C., Li, K.-M., Higginbotham, S., Rogan, E. G., and Cavalieri, E. L. (1994) Synthesis and tumor-initiating activity in mouse skin of dibenzo[*a,l*]pyrene *syn*- and *anti*-fjord-region diol epoxides. *Carcinogenesis* **15**, 2455−2460.

(11) Ralston, S. L., Lau, H. H. S., Seidel, A., Luch, A., Platt, K. L., and Baird, W. M. (1994) The potent carcinogen dibenzo[*a,l*]pyrene is metabolically activated to fjord-region 11,12-diol 13,14-epoxides in human mammary carcinoma MCF-7 cell cultures. *Cancer Res.* **54**, 887−890.

(12) Li, K.-M., RamaKrishna, N. V. S., Padmavathi, N. S., Rogan, E. G., and Cavalieri, E. L. (1994) Synthesis and structure determination of the adducts of dibenzo[*a,l*]pyrene diol epoxides and deoxyadenosine and deoxyguanosine. *Polycycl. Aromat. Compd.* **6**, 207−213.

(13) Devanesan, P. D., Rogan, E. G., and Cavalieri, E. L. (1995) Identification of stable DNA adducts of dibenzo[*a,l*]pyrene. *Proc. Am. Assoc. Cancer Res.* **36**, 137.

(14) Cavalieri, E. L., and Rogan, E. G. (1992) The approach to understanding aromatic hydrocarbon carcinogenesis. The central role of radical cations in metabolic activation. *Pharmacol. Ther.* **55**, 183−199.

(15) Jankowiak, R., and Small, G. J. (1991) Fluorescence line narrowing: a high-resolution window on DNA and protein damage from chemical carcinogens. *Chem. Res. Toxicol.* **4**, 256−269.

(16) Rogan, E. G., Devanesan, P. D., RamaKrishna, N. V. S., Higginbotham, S., Padmavathi, N. S., Chapman, K., Cavalieri, E. L., Jeong, H., Jankowiak, R., and Small, G. J. (1993) Identification and quantitation of benzo[*a*]pyrene-DNA adducts formed in mouse skin. *Chem. Res. Toxicol.* **6**, 356−363.

(17) Devanesan, P. D., RamaKrishna, N. V. S., Padmavathi, N. S., Higginbotham, S., Rogan, E. G., Cavalieri, E. L., Marsh, G. A., Jankowiak, R., and Small, G. J. (1993) Identification and quantitation of 7,12-dimethylbenz[*a*]anthracene-DNA adducts formed in mouse skin. *Chem. Res. Toxicol.* **6**, 364−371.

(18) Kok, S. J., Posthumus, R., Bakker, I., Gooijer, C., Brinkman, U. A. Th., and Velthorst, N. H. (1995) Identification of benzo[*a*]-pyrene tetrols by reversed-phase liquid chromatography coupled

semi-on-line to fluorescence line-narrowing spectroscopy. *Anal. Chim. Acta* **303**, 3−10.
(19) Marsh, G. A., Jankowiak, R., Suh, M., and Small, G. J. (1994) Sequence dependence of benzo[*a*]pyrene diol epoxide-DNA adduct conformer distribution: a study by laser-induced fluorescence/polyacrylamide gel electrophoresis. *Chem. Res. Toxicol.* **7**, 98−109.
(20) Suh, M., Jankowiak, R., Ariese, F., Mao, B., Geacintov, N. E., and Small, G. J. (1994) Flanking base effects on the structural conformation of the (+)-*trans*-*anti*-benzo[*a*]pyrene diol epoxide adduct to N^2-dG in sequence-defined oligonucleotides. *Carcinogenesis* **15**, 2891−2898.
(21) Suh, M., Ariese, F., Small, G. J., Jankowiak, R., Liu, T.-M., and Geacintov, N. E. (1995) Conformational studies of the (+)-*trans*-, (-)-*trans*-, (+)-*cis*-, and (-)-*cis* adducts of *anti*-benzo[*a*]pyrene diol epoxide to N^2-dG in duplex oligonucleotides using polyacrylamide gel electrophoresis and low-temperature fluorescence spectroscopy. *Biophys. Chem.* **56**, 281−296.
(22) Ariese, F., Small, G. J., and Jankowiak, R. (1996) Conformational studies of depurinating DNA adducts from *syn*-dibenzo[*a*,*l*]pyrene diol epoxide. *Carcinogenesis* **17**, 829−837.
(23) Rodriguez, H., and Loechler, E. L. (1993) Mutagenesis by the (+)-*anti* diol-epoxide of benzo[*a*]pyrene: what controls mutagenic specificity? *Biochemistry* **32**, 1759−1769.
(24) Shibutani, S., Margulis, L. A., Geacintov, N. E., and Grollman, A. (1993) Translesional synthesis on a DNA template containing a single stereoisomer of dG-(+)- or dG-(-)-*anti*-BPDE (7,8-dihydroxy-*anti*-9,10-epoxy-7,8,9,10-tetrahydrobenzo[*a*]pyrene). *Biochemistry* **32**, 7531−7541.
(25) Suh, M., Ariese, F., Small, G. J., Jankowiak, R., Hewer, A., and Phillips, D. H. (1995) Formation and persistence of benzo[*a*]pyrene-DNA adducts in mouse epidermis *in vivo*: importance of adduct conformation. *Carcinogenesis* **16**, 2561−2569.
(26) Bushman, D. R., Grossman, S. J., Jerina, D. M., and Lehr, R. E. (1989) Synthesis of optically active fjord-region 11,12-diol 13,14-epoxides and the K-region 9,10-oxide of the carcinogen benzo[*g*]-chrysene. *J. Org. Chem.* **54**, 3533−3544.
(27) Burkert, U., and Allinger, N. L. (1982) *Molecular mechanics*, ACS Monograph Vol. 177, American Chemical Society, Washington, DC.
(28) Allinger, N. L. (1977) Conformational analysis 130. MM2: a hydrocarbon force field utilizing V1 and V2 torsional terms. *J. Am. Chem. Soc.* **99**, 8127−8134.
(29) Ridley, J. E., and Zerner, M. C. (1976) Triplet states via intermediate neglect of differential overlap: benzene, pyridine, and the diazines. *Theoret. Chim. Acta* **42**, 223−236.
(30) Del Bene, J., and Jaffé, H. H. (1968) Use of the CNDO method in spectroscopy I. benzene, pyridine, and the diazines. *J. Chem. Phys.* **48**, 1807−1813.
(31) Del Bene, J., and Jaffé, H. H. (1968) Use of the CNDO method in spectroscopy II. five-membered rings. *J. Chem. Phys.* **48**, 4050−4055.
(32) Brown, J. C. (1982) Ph.D. Thesis, Iowa State University, Ames, IA.
(33) Brown, J. C., Duncanson, J. A., and Small, G. J. (1980) Fluorescence line narrowing spectrometry in glasses for direct determination of polycyclic aromatic hydrocarbons in solvent-refined coal. *Anal. Chem.* **52**, 1711−1715.
(34) Herzberg, G. (1966) Molecular Spectra and Molecular Structure, III. *Electronic Spectra and Electronic Structure of Polyatomic Molecules*, Chapter II, van Nostrand and Reinhold Co., New York.
(35) Gordon, A. J., and Ford, R. A. (1972) *The Chemist's Companion; a Handbook of Practical Data, Techniques, and References*; John Wiley & Sons, New York.

TX960211A